Proceedings of the 10th Brazilian Congress of Thermal Sciences and Engineering – ENCIT 2004
Braz. Soc. of Mechanical Sciences and Engineering – ABCM, Rio de Janeiro, Brazil, Nov. 29 – Dec. 03, 2004

Paper CIT04-0531

On The Effect of Convective Flux Computation Schemes on Boundary Layer Flows

Enda Dimitri Vieira Bigarella
Instituto Tecnológico de Aeronáutica, São José dos Campos, SP, BRAZIL - 12228-900
enda_bigarella@yahoo.it

Farney Coutinho Moreira
Instituto Tecnológico de Aeronáutica, São José dos Campos, SP, BRAZIL - 12228-900
farney@ita.br

João Luiz F. Azevedo
Centro Técnico Aeroespacial, São José dos Campos, SP, BRAZIL - 12228-904
azevedo@iae.cta.br

Abstract. *This paper presents the effects of some convective flux computation schemes on boundary layer flow solutions. For such study, centred and upwind convective flux computation schemes will be discussed. The centred method considered is the second-order accurate Jameson scheme plus explicitly added artificial dissipation terms. Three artificial dissipation models, namely a scalar and a matrix version of a switched model, and the CUSP model, are considered in the paper. For the upwind method, the second-order accurate Roe flux-difference splitting scheme is used. It has been observed that the explicitly added artificial dissipation terms of the centred scheme may play an important role on the modification of the correct flow solution, whereas upwind schemes seem to correctly represent the flow structure. This aspect will be carefully addressed and discussed in the paper. A flat plate configuration is used to address the influence of artificial dissipation terms, added either explicitly or naturally available in the flux computation scheme, in boundary layer flows. Theoretical solution for this test case is available, which is used to assess the numerical results obtained.*

keywords: *CFD, boundary layers, flux computation*

1. Introduction

Many approaches are available in the literature to numerically simulate aerodynamic flows over aerospace configurations. The CFD group at Instituto de Aeronáutica e Espaço (IAE) already achieved good results using both finite difference on structured grids and finite volume techniques on unstructured grids. This paper discusses the results obtained using a finite volume method on 3-D unstructured meshes, which has already been used to simulate turbulent viscous flows over typical aerospace configurations (Bigarella et al., 2003).

The computational code solves the Reynolds-averaged Navier-Stokes (RANS) equations. A fully explicit, 2nd-order accurate, 5-stage, Runge-Kutta time stepping scheme is used to perform the time marching of the flow equations. Boundary conditions are set through the use of ghost cells attached to the boundary faces. The implementation uses a cell-centred, face-based data structure and the code can use meshes with any combination of tetrahedra, hexahedra, triangular-base prisms and pyramids. Extensive validation of this numerical code had already been initiated and one is referred to Scalabrin, 2002 for a careful analysis of the initial validation results. The main interest in the present paper is to assess possible flux calculation methods suitable for the typical aerospace applications of interest for the present CFD group. For flux computations on the volume faces, a second-order accurate Jameson centred scheme (Jameson et al., 1981) and a second-order accurate Roe upwind flux-difference splitting method (Roe, 1981) can be used. In the centred case, explicit addition of artificial terms is required to control nonlinear instabilities in the numerical solution. For computation of artificial dissipation terms in this case, both a scalar and a matrix version of a switched second- and fourth-difference model are available (Mavriplis, 1990; Turkel and Vatsa, 1994). The Convective Upwind Split Pressure (CUSP) artificial dissipation model (Jameson, 1995a; Jameson, 1995b) is also considered in the centred scheme case.

Subsonic laminar flows about a flat plate configuration are used to study the effect of the numerical flux computation schemes in boundary layer flows. It is known that some schemes may have some influence in boundary layer flow solutions, as reported in Allmaras, 2002; Swanson et al., 1998; Zingg et al., 1999; Bigarella, 2002. The latter reference, in particular, is a work developed by the present CFD group in a finite-difference code

context. In that reference, an abnormal behaviour of the numerically obtained boundary layer, when compared to the expected theoretical Blasius profile, has been reported. In that document, the present group claims that such problems are due to non-physical behaviour of the centred flux computation scheme, more precisely in the explicitly added artificial dissipation model, and to an inconsistent computational mesh configuration. Similar problems have already been obtained with the present finite volume code and the present paper shows conclusive results that corroborate the previous assertive.

2. Theoretical Formulation

The flows of interest for the present CFD group are modelled by the 3-D compressible Reynolds-averaged Navier-Stokes (RANS) equations. These equations can be written in dimensionless form, assuming a perfect gas, as

$$\frac{\partial Q}{\partial t} + \frac{\partial E_e}{\partial x} + \frac{\partial F_e}{\partial y} + \frac{\partial G_e}{\partial z} = \frac{\partial E_v}{\partial x} + \frac{\partial F_v}{\partial y} + \frac{\partial G_v}{\partial z} \ , \tag{1}$$

where Q is the dimensionless vector of conserved variables, defined as

$$Q = \left[\begin{array}{cccc} \rho & \rho u & \rho v & \rho w \end{array} \right. \left. \begin{array}{c} e \end{array} \right]^{\mathrm{T}} \ . \tag{2}$$

Here, ρ is the fluid density, u, v and w are the Cartesian velocity components and e is the fluid total energy per unit of volume. The formulation for the dimensionless inviscid flux vectors, E_e, F_e and G_e, and the dimensionless viscous flux vectors E_v, F_v and G_v, as well as other definitions in Eq. (1) can be found in Bigarella et al., 2004.

The main interest of the present CFD group is high-Reynolds number simulations of flows over complex aerodynamic configurations. Such applications require adequate turbulence closures in order to correctly account for the large transport effects of the turbulence at such flight conditions. Two turbulence closures have been chosen in the present context, namely, the Spalart-Allmaras (Spalart and Allmaras, 1992) (SA) one-equation model and the Menter SST (Menter and Grotjans, 1998) two-equation model. Both closures are particularly suited for aerodynamic flow simulations and separation prediction (Menter and Grotjans, 1998). Furthermore, they are also less restrictive in relation to the grid refinement near the wall than other two-equation models such as the $k - \epsilon$ family of models (Menter and Grotjans, 1998). Implementation details on this formulation and numerical results can be found in Scalabrin, 2002 and Bigarella et al., 2003.

3. Numerical Formulation

The finite volume method is used to obtain the solution of the RANS equations. The formulation of the method is obtained by an integration of the flow equations in a finite volume. The application of Gauss theorem for each finite volume yields, for an elementary volume and assuming a stationary mesh

$$\frac{\partial Q_i}{\partial t} = -\frac{1}{V_i} \sum_{k=1}^{nf} \left[\vec{P}_{e_k} - \vec{P}_{v_k} \right] \cdot \vec{S}_k \ , \qquad \vec{P} = E\,\hat{\imath}_x + F\,\hat{\imath}_y + G\,\hat{\imath}_z \ , \tag{3}$$

where nf is the number of faces which form the control volume and $\vec{S}_k$ is the outward oriented normal area vector of the k-th face. The discrete value of the vector of conserved variables for the i-th control volume is defined as the mean value of the conserved variables in the volume. The code is able to simulate flows on grids comprised of tetrahedra, hexahedra, triangular-base prisms, pyramids or a mix of these types of elements. The previous equation also indicates that the integral was discretized assuming the fluxes to be constant on the faces.

4. Time Integration and Multigrid

Time integration of Eq. (3) is performed using a Runge-Kutta type scheme similar to the one proposed in Jameson et al., 1981. In the present work, a 2nd-order accurate, 5-stage Runge-Kutta scheme is used. The time step for each volume is calculated assuming a constant CFL number throughout the computational domain. More details on this formulation can be found in Scalabrin, 2002 and Bigarella et al., 2004.

A multigrid scheme is also available in the present numerical code in order to accelerate convergence to steady-state. The chosen multigrid algorithm is of a full approximation storage (FAS) type, which is the recommended method for nonlinear problems (Fletcher, 1988). This method is based on exchanging both solution and residue values between different grid levels. It also relies on a good time marching procedure to be effective. This method has been successfully validated within the present 3-D unstructured computational code for inviscid to turbulent viscous simulations, as shown in Bigarella et al., 2003. In order to improve the multigrid algorithm as well as the computational method, the simulations start at the coarsest grid level. Some iterations with the Runge-Kutta time stepping are performed at this grid and a high-order interpolation is performed to the next

finer grid. Some multigrid cycles are, then, performed to improve the solution at this grid. This procedure is repeated successively until the finest grid is reached, with a good initial guess to the solution. Multigrid cycles are, then, performed on the finest mesh until convergence is reached. This technique is usually denominated as a full multigrid (FMG) method. The coarse mesh levels used by the multigrid scheme are generated with an agglomeration technique. More details on the multigrid algorithm as well as the agglomeration technique can be found in Bigarella et al., 2004.

5. Spatial Discretization

Both centred and upwind schemes are available in the present numerical method for computation of convective fluxes. Viscous fluxes are always computed by a second-order accurate centred scheme in the present paper.

5.1. Centred Scheme

The centred scheme used in this work for spatial discretization of the convective fluxes was proposed in Jameson et al., 1981. For this scheme, the convective operator, CO_i, is calculated as the sum of the inviscid fluxes on the faces of the i-th volume

$$CO_i = \sum_{k=1}^{nf} \vec{P}_e\left(Q_k\right) \cdot \vec{S}_k \ , \qquad Q_k = \frac{1}{2}\left(Q_i + Q_m\right) . \tag{4}$$

In this expression, Q_i and Q_m are the conserved properties in the volumes at each side of the k-th face and m indicates the neighbour of the i-th element.

5.2. Artificial Dissipation Schemes

Centred schemes require the explicit addition of artificial dissipation terms in order to control nonlinear instabilities that may arise in the flow simulation. Several models to compute the artificial terms are included in the present numerical formulation. A description of the available models is presented in the forthcoming sections.

5.2.1. Mavriplis Scalar Switched Model (MAVR)

The artificial dissipation operator is built by a switch of undivided Laplacian and bi-harmonic operators. In regions of high property gradients, the bi-harmonic operator is turned off in order to avoid oscillations. In smooth regions, the undivided Laplacian operator is turned off in order to maintain 2nd order accuracy. A numerical pressure sensor is responsible for this switching between the operators. The expression for the artificial dissipation operator, DI_i, is given by

$$DI_i = \sum_{m=1}^{nb} \left\{ \left(\frac{A_m + A_i}{2} \right) \left[\ \epsilon_2 \left(Q_m - Q_i\right) - \epsilon_4 \left(\nabla^2 Q_m - \nabla^2 Q_i\right) \ \right] \right\} , \tag{5}$$

where m represents the neighbours of the i-th element and nb is the total number of neighbours of the i-th control volume. Furthermore,

$$\nabla^2 Q_i = \sum_{m=1}^{nb} \left[Q_m - Q_i\right] \ , \ \ \epsilon_2 = K_2 \max\left(\nu_i, \nu_m\right) \ , \ \ \epsilon_4 = \max\left(0, K_4 - \epsilon_2\right) \ , \ \ \nu_i = \frac{\sum_{m=1}^{nb} \left|p_m - p_i\right|}{\sum_{m=1}^{nb} \left[p_m + p_i\right]} \ . \tag{6}$$

In this work, K_2 and K_4 are assumed equal to $1/4$ and $3/256$, respectively. The A_i coefficient calculation is described in Mavriplis, 1988 and Mavriplis, 1990. The expression for the coefficients is

$$A_i = \sum_{k=1}^{nf} s_k \ , \qquad s_k = \left| \vec{q}_k \cdot \vec{S}_k \right| + a_k \left| \vec{S}_k \right| \ , \tag{7}$$

in an attempt to obtain steady state solutions which are independent of the time step (Azevedo, 1992).

5.2.2. Matrix Switched Model (MATD)

The formulation for the matrix model is similar to the previously described one for the MAVR model, except for the definition of the A_i terms. In this case, the Jacobian flux matrices, as defined in Turkel and Vatsa, 1994,

are used instead of the scalar term inside the summation in Eq. (7). The A_i term in Eq. (7), re-interpreted for the present cell-centred, face-based finite-volume framework, can be written as

$$s_k = |\lambda_3| I + \left[\frac{|\lambda_1| + |\lambda_2|}{2} - |\lambda_3|\right]\left(\frac{\gamma-1}{a_k^2}E_1 + \frac{1}{|\vec{S}_k|}E_2\right) + \frac{|\lambda_1| - |\lambda_2|}{2a_k}\left[E_3 + (\gamma-1)\,E_4\right] \ . \tag{8}$$

In this equation, the following definitions are used

$$\begin{aligned} |\lambda_1| &= \max(\left|\vec{q}_k \cdot \vec{S}_k + a_k\,|\vec{S}_k|\right|,\ V_n\lambda)\ , \qquad |\lambda_2| = \max(\left|\vec{q}_k \cdot \vec{S}_k - a_k\,|\vec{S}_k|\right|,\ V_n\lambda)\ , \\ |\lambda_3| &= \max(\left|\vec{q}_k \cdot \vec{S}_k\right|,\ V_l\lambda)\ , \qquad \lambda = \left|\vec{q}_k \cdot \vec{S}_k\right| + a_k\,|\vec{S}_k|\ . \end{aligned} \tag{9}$$

Furthermore, in these expressions V_n limits the eigenvalues associated with the nonlinear characteristic fields whereas V_l provides a similar limiter for the linear characteristic fields. Such limiters are used near stagnation and/or sonic lines, where the eigenvalues approach zero, in order to avoid zero artificial dissipation. The recommended values (Turkel and Vatsa, 1994) for these limiters, $V_n = 0.25$ and $V_l = 0.025$, are used in the present effort. Furthermore,

$$E_1 = R_1^T R_2\ , \qquad E_2 = R_3^T R_4\ , \qquad E_3 = R_1^T R_4\ , \qquad E_4 = R_3^T R_2\ . \tag{10}$$

where

$$\begin{aligned} R_1 &= \{1, u, v, w, h,\}\ , \qquad R_2 = \left\{\frac{1}{2}|\vec{q}|^2, -u, -v, -w, 1,\right\}\ , \\ R_3 &= \left\{0, S_x, S_y, S_z, \vec{q}\cdot\vec{S},\right\}\ , \qquad R_4 = \left\{-\vec{q}\cdot\vec{S}, S_x, S_y, S_z, 0,\right\}\ . \end{aligned} \tag{11}$$

In the previous equations, $h = (e+p)/\rho$ is the enthalpy and the area vector is defined as $\vec{S} = \{S_x, S_y, S_z\}$. For the MATD artificial dissipation model, in order to get a fully upwind scheme in supersonic regions, the recommended value for the K_2 constant is $K_2 = 1/2$.

5.2.3. Convective Upwind and Split Pressure Scheme (CUSP)

Previously, the scalar and matrix-valued artificial dissipation terms have been constructed considering differentials in the conserved property array. For the CUSP model (Jameson, 1995a; Jameson, 1995b; Swanson et al., 1998), the artificial dissipation terms are instead chosen as a linear combination of the conserved property array and the flux vectors. The second-order accurate CUSP model artificial dissipation term in an interface is re-interpreted for the present cell-centred, face-based finite volume framework as follows

$$DI_i = \sum_{k=1}^{nf} d_k\ , \qquad d_k = \frac{1}{2}\alpha^* a_k |\vec{S}_k|\,(Q_R - Q_L) + \frac{1}{2}\beta\left(\vec{P}_{e_R} - \vec{P}_{e_L}\right)\cdot\vec{S}_k\ , \qquad \alpha^* = \alpha - \beta M_n\ , \tag{12}$$

where $\vec{P}$ is defined in Eq. (3) and

$$\alpha = \begin{cases} |M_n| & \text{if } |M_n| \geq \epsilon \\ \frac{1}{2}\left(\epsilon + \frac{M_n^2}{\epsilon}\right) & \text{if } |M_n| < \epsilon \end{cases}\ , \qquad \beta = \text{sign}(M_n)\min\left(1, \max\left(0, \frac{|\bar{q}_n| + |q_n| - a}{|\bar{q}_n| - |q_n| + a}\right)\right)\ . \tag{13}$$

In these equations, $M_n = \bar{q}_n/a$ is the Mach number in the face normal direction, computed as $q_n = \vec{q}\cdot\vec{S}$, and ϵ is a threshold in order to avoid zero artificial dissipation near stagnation lines, chosen as $\epsilon = 10^{-8}$ in this work. It is important to remark here that face properties are computed using the Roe average procedure (Roe, 1981; Swanson et al., 1998), except for $\bar{q}$, which is computed by an arithmetic average in the face.

5.3. Upwind Roe Flux-Difference Splitting Scheme (fROE)

The upwind discretization in the present context is performed by the Roe flux-difference splitting method (Roe, 1981). For this scheme, the numerical flux in the k-th face can be written as

$$\overline{E}_{ek} = \frac{1}{2}\left[E_{e_L} + E_{e_R} - \left|\widetilde{A}\right|(Q_L - Q_R)\right]\ . \tag{14}$$

which results in

$$CO_i = \sum_{k=1}^{nf}\left(\overline{E}_{ek}\,\hat{\imath}_x + \overline{F}_{ek}\,\hat{\imath}_y + \overline{G}_{ek}\,\hat{\imath}_z\right)\cdot\vec{S}_k\ , \qquad DI_i = 0\ . \tag{15}$$

It can be shown that

$$\left|\widetilde{A}\right|(Q_R - Q_L) = \sum_{\ell} |\lambda_\ell|\, \alpha_\ell r_\ell \ , \tag{16}$$

where λ_ℓ is the ℓ-th eigenvalue related to the Euler equations, r_ℓ is the corresponding eigenvector and α_ℓ is the projection of the property jump at the interface over vector r_ℓ. Properties in the volume faces are computed using the Roe average procedure, as detailed in Roe, 1981. The cited reference also presents the definitions for the r_ℓ and α_ℓ terms in the previous formulation.

5.4. MUSCL Reconstruction

To achieve 2nd order accuracy in space for the CUSP and fROE schemes, linear distributions of properties are assumed at each cell to compute the left and right states in the face. Such states are represented by the L and R subscripts, respectively, in the CUSP and fROE definitions.

The linear reconstruction of properties is achieved through a MUSCL (van Leer, 1979) scheme, in which the property at the interface is obtained through a limited extrapolation using the cell properties and their gradients. The expressions for the reconstructed properties in the control volume faces can be written as

$$q_L = q_i + \psi^- \nabla q_i \cdot \vec{r}_i \ , \qquad q_R = q_m + \psi^+ \nabla q_m \cdot \vec{r}_m \ , \tag{17}$$

where ∇q_i and ∇q_m are the gradients computed for the i-th cell and its neighbouring m-th cell, respectively; $\psi^\pm$ represent the limiters; and $\vec{r}_i$ and $\vec{r}_m$ are the distance vectors from the i-th and m-th cell centroids, respectively, to the face centroid.

The *minmod* limiter (Hirsch, 1991) is used in the present context. The extension of the 1-D limiter, as defined in Hirsch, 1991, to the 3-D case is based on the work of Barth and Jespersen, 1989 and Azevedo et al., 2001. For each n-th vertex of the i-th cell, the property $q_{i_n} = q\,(x_n, y_n, z_n)$ in that vertex is reconstructed as

$$q_{i_n} = q_i + \nabla q_i \cdot \vec{r}_n \ , \tag{18}$$

where $\vec{r}_n$ is the distance of the n-th vertex of the i-th cell to the centroid of this cell. A limiter is computed at each vertex of the control volume. For the *minmod* limiter, this quantity is given by

$$\overline{\psi}_{i_n} = \begin{cases} \min\left(1, \frac{q_i^{\max} - q_i}{q_{i_n} - q_i}\right) & ,\text{if } q_{i_n} - q_i > 0 \ , \\ \min\left(1, \frac{q_i^{\min} - q_i}{q_{i_n} - q_i}\right) & ,\text{if } q_{i_n} - q_i < 0 \ , \\ 1 & ,\text{if } q_{i_n} - q_i = 0 \ . \end{cases} \tag{19}$$

The limiter value for the i-th control volume is finally obtained as

$$\psi_i = \min\left(\overline{\psi}_{i1}, \overline{\psi}_{i2}, ..., \overline{\psi}_{inbmax}\right) \ , \tag{20}$$

where $nbmax$ is the total number of nodes of the i-th control volume.

5.5. Viscous Flux Computation

The Navier-Stokes viscous terms are computed by a second-order accurate centred scheme. The viscous operator in the i-th control volume is calculated as the sum of the viscous fluxes on the faces which constitute the volume. In this case, both the conserved variable vector and the derivatives on the face, used to compute the viscous terms, are calculated as the arithmetic average between these quantities in the two volumes which contain the face. Derivatives of flow variables, for each control volume, are calculated in the standard finite volume approach in which these derivatives are transformed, by the gradient theorem, into surface integrals around the control volume (Swanson and Radespiel, 1991; Azevedo et al., 1999).

6. Results and Discussion

For this study, subsonic laminar flows about a flat plate configuration, with Reynolds number $Re = 10^5$ and Mach number $M_\infty = 0.254$, are considered. The present effort has been motivated by an anomaly in the boundary layer of subsonic laminar flows about a flat plate configuration. More precisely, this anomaly has been observed by the present CFD group in the bend of the boundary layer profile (Bigarella, 2002). Extensive numerical tests led to the conclusion that this issue may be related to inherent problems in the formulation of the explicitly added artificial dissipation terms for the centred flux computation scheme. A dependency of the numerical solution with the computational mesh topology and density has also been observed. This problem has been encountered in another context, namely in a finite difference code. A simple demonstration of the

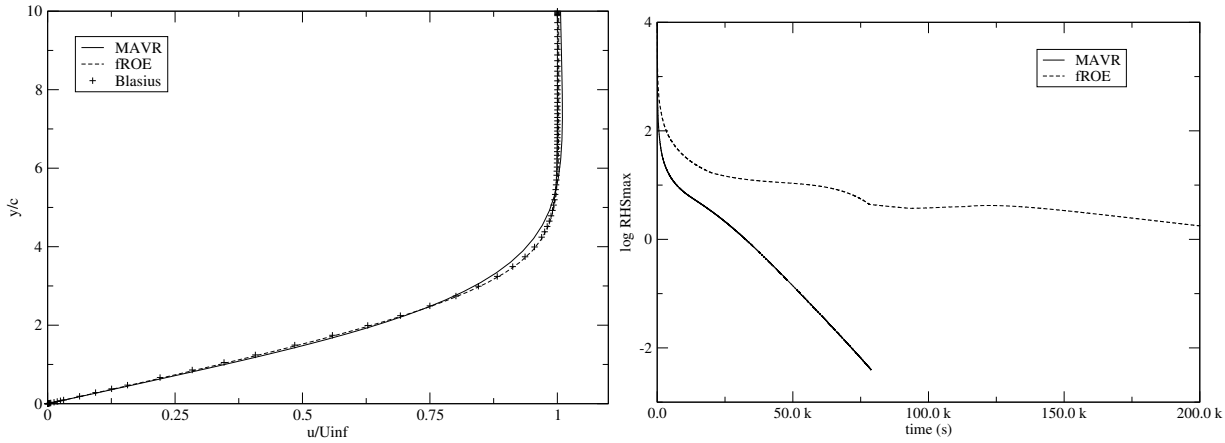

(a) Boundary layers.

(b) Residue histories.

Figure 1: Flat plate laminar boundary layer results obtained with the MAVR ($CFL = 2.0$) and the fROE ($CFL = 1.5$) schemes.

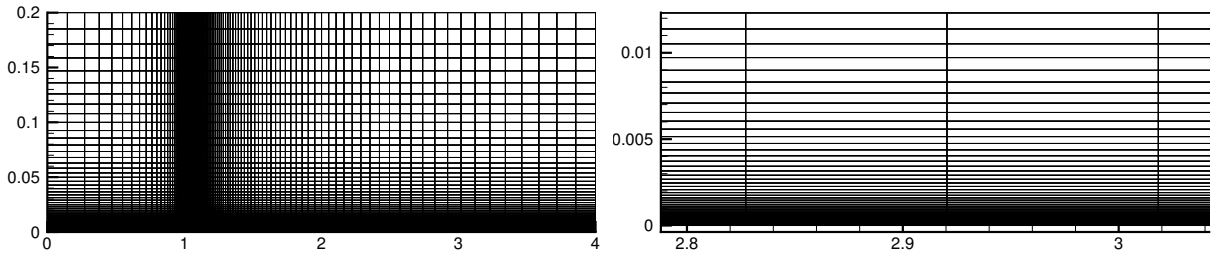

(a) Full view.

(b) Detail.

Figure 2: 2-D views of the original grid for a flat plate flow.

relation of this problem to the artificial dissipation formulation has also been discussed in Bigarella, 2002. The first obvious test to ascertain whether the centred flux computation scheme was related to the previously described problem was to perform a similar simulation with an upwind scheme. Nevertheless, such an upwind flux computation scheme was not available in that code and further tests regarding the artificial dissipation terms could not be performed.

Similar problems, however, have also been found in the present finite volume code for the MAVR centred scheme, as presented in Fig. 1. An oscillation of the numerical solution for the MAVR model in the bend of the boundary layer profile can clearly be observed. Similar results for the upwind fROE scheme are also available in this figure. It can be observed that the upwind solution is very close to the Blasius boundary layer, without any oscillation, which is indicative that the problem in the bend of the boundary layer profile is related to the flux computation scheme, as initially postulated.

The grid used in the previous results is constructed by a very simple exponential growth along the normal direction, equal at every longitudinal station. This grid has 121 points along the longitudinal direction and 89 in the normal one, which sums up to 10560 volumes in the grid, and the exponential growth ratio along the normal direction is 8%. The plate chord length is 3 units, and the grid extends one unit upstream and 0.2 unit in the normal direction. A view of such grid can be found in Fig. 2. In this grid, the plate starts at $x = 1$. The grid is also clustered near the flat plate leading edge in order to account for the large gradients that are expected in this region.

Another important aspect concerning this test case regards the usage of computational resources by this computational grid. In Fig. 1, residue histories for both centred and upwind schemes can be found for simulations carried on a 2.0 GHz Pentium-IV PC. The maximum residue of the continuity equation is plotted in this figure. It can clearly be observed that very large computational times are necessary for convergence to an engineering

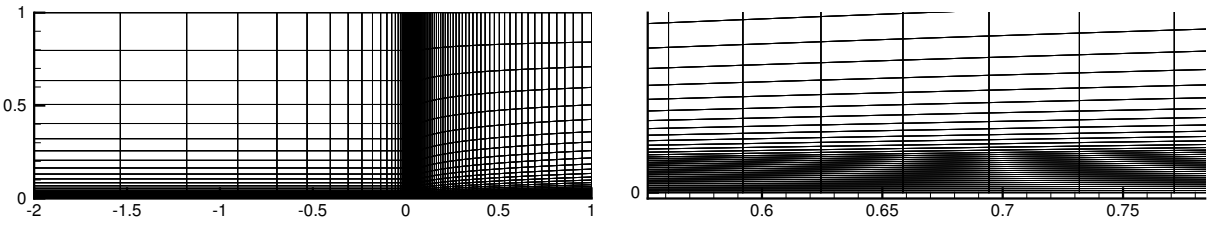

(a) Full view.

(b) Detail.

Figure 3: 2-D views of the new grid over a flat plate with 20 points inside the boundary layer.

level of accuracy. This behaviour may be explained by some undesired characteristics observed in the previously described grid, such as:

- The same grid spacing in the normal direction along every flat plate longitudinal station, which results in different number of cells inside the boundary layer along the longitudinal direction;
- Large stretching along the normal direction in order to try to provide a sufficient number of points inside the boundary layer;
- Very large number of cells in the computational grid in order to try to provide a sufficient number of points inside the boundary layer;
- The external boundaries are very close to the plate.
- Absence of a sufficient number of points in the bend of the boundary layer, where the viscous region bends to conform to the outer potential flow, and where, thus, considerable gradients are expected.

These grid characteristics lead to slow convergence rates, as observed in Fig. 1, due to large grid stiffness, and also due to large computational resources consumption because of the large number of control volumes in the mesh. This situation becomes worse for the upwind case, to which the convergence is much slower, and the computational costs per iteration increase by a factor of 5. The numerical result for this simulation, however, is very close to the theoretical one, even at such relatively high residue level as, seen in Fig. 1.

A more suitable computational mesh, which solves the previously described problems, can be obtained. The corresponding mesh generator places a user-provided number of computational cells inside the boundary layer. These cells are evenly spaced along the normal direction and they extend to a user-defined height, given by a Blasius-transformed length, which is defined as $\eta = \frac{y}{x}\sqrt{Re_x}$. This height varies with the longitudinal position, following the theoretical growth of the boundary layer up to the value of η. This grid construction allows the user to keep a constant number of points inside the boundary layer along the flat plate length. The automatic exponential growth guarantees the normal direction length and a sufficiently low number of cells outside the constant grid spacing of the boundary layer. This specific grid construction requires the knowledge of the flow Reynolds number, which should correctly be provided by the user. The plate length is fixed as one and the grid extends two lengths upstream the plate leading edge and one length along the normal direction. One quarter of the number of points specified by the user for the longitudinal direction is placed in the two-length space ahead the plate, and the resulting number of points is placed along the plate longitudinal direction. These points are clustered near the flat plate leading edge in order to account for the larger gradients that are expected in this region.

Three grids have been generated with this mesh generator for the previously described subsonic flat plate flow. Different number of cells inside the boundary layer, namely 10, 20 and 40 points, are considered, with 30 cells outside the boundary layer. The user-defined boundary layer height in terms of the Blasius transformed coordinate is $\eta = 6$. All grids have 81 points along the longitudinal direction. These grids have less than half the number of cells of the original grid, with much less stretching inside the boundary layer, which is expected to guarantee faster convergence rates for the simulations. A view of the grid with 20 points inside the boundary layer can be found in Fig. 3.

Figure 4 presents boundary layer results obtained with the previously described computational grids. Centred and upwind scheme results have been considered in this figure, and they are compared to the theoretical Blasius solution. It is interesting to observe that the upwind fROE scheme and the MATD and CUSP models guarantee the correct solution with all tested grid configurations. The MAVR centred scheme presents an anomaly in

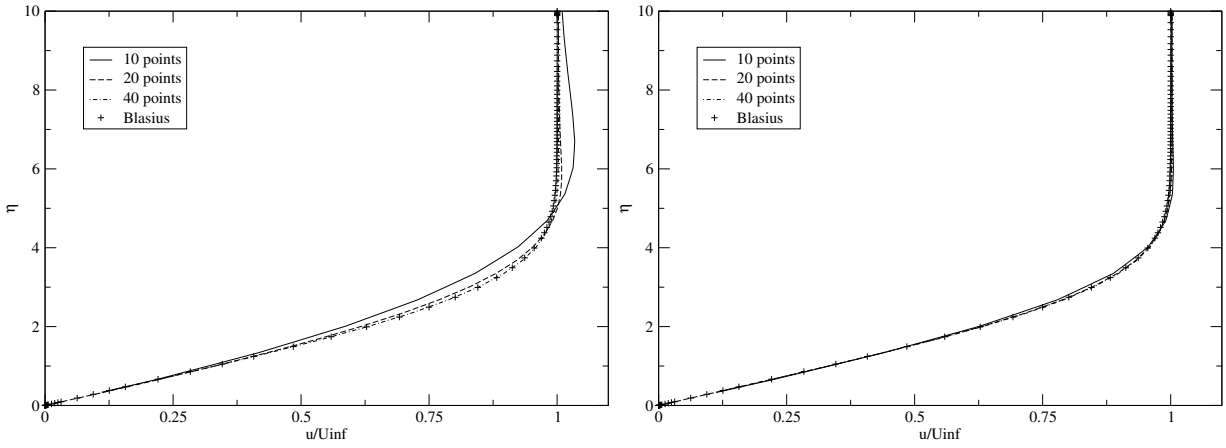

(a) MAVR model.

(b) MATD model.

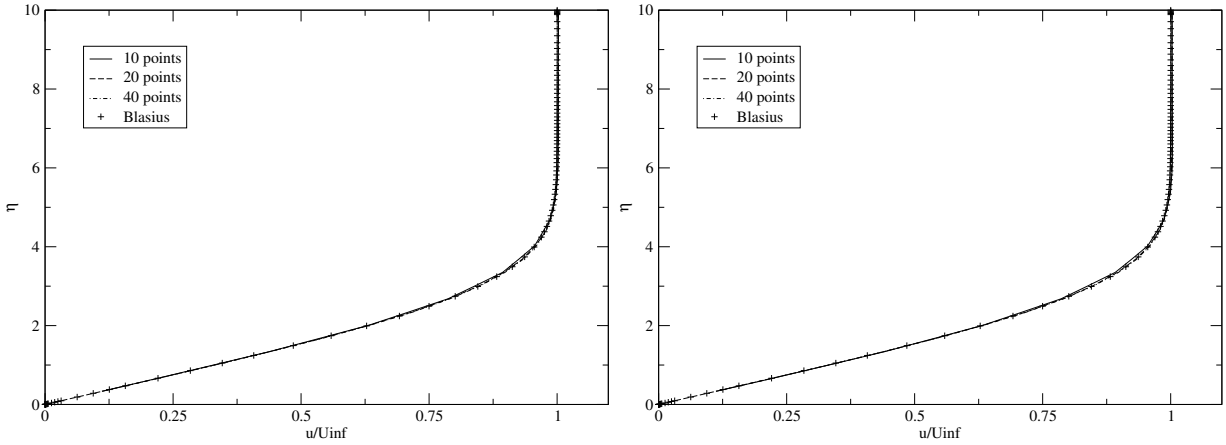

(c) CUSP model.

(d) fROE scheme.

Figure 4: Laminar boundary layers over a flat plate obtained with different flux computation schemes and computational grids.

the bend of the boundary layer profile for the grids with a smaller number of points in the layer, as already verified. The oscillation, nevertheless, decreases with the increasing number of such points. With the 40-point grid configuration, the correct solution can be obtained with the MAVR model.

In terms of computational resource usage, these new grid configurations are much cheaper than the original computational mesh. Figure 5 presents corresponding residue histories for the previously described simulations. In this figure, one can clearly observe the increase in the computational time with the increasing number of points. It is also interesting to observe that, in terms of one iteration of MAVR, the MATD model is about 4 times more expensive, whereas the CUSP is twice and the fROE is about five. Nevertheless, all models but MAVR presented consistent and unvarying boundary layer solutions throughout all the grid configurations tested. Furthermore, even for the most expensive case in Fig. 5, these simulations are much cheaper than the ones considered in Fig. 2. This result, along with the ones presented in Fig. 4, corroborate the previous assertive that grid density and topology have a strong influence in both numerical solution accuracy and convergence. A suitable grid configuration has been obtained to which computational results and convergence are acceptable.

7. Concluding Remarks

The paper presents results obtained with a finite volume code developed to solve the RANS equations over aerospace configurations. The code uses a Runge-Kutta type scheme to perform time marching. The fluxes on the volume faces are computed by either a centred scheme plus explicitly added artificial dissipation terms or a 2nd order flux-difference splitting upwind scheme. Three artificial dissipation models are considered to include

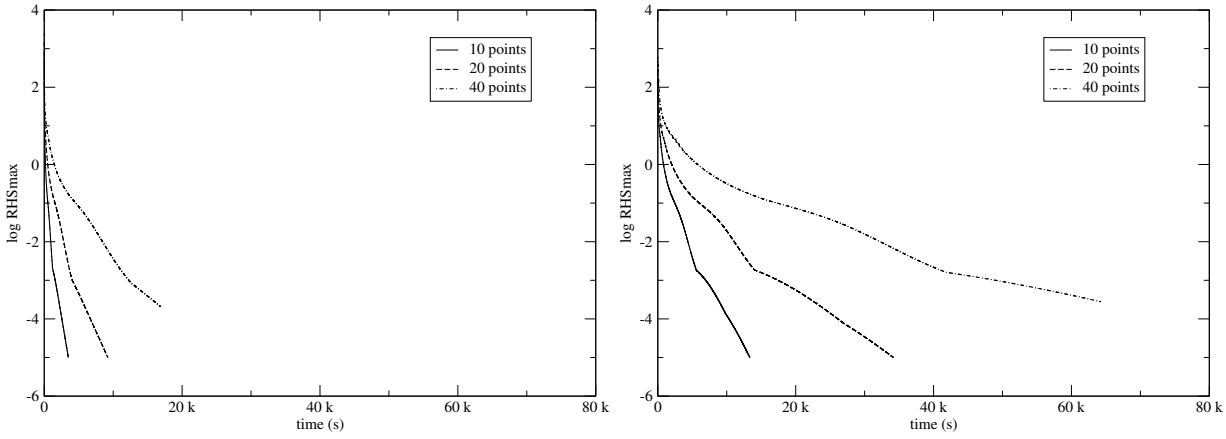

(a) MAVR model ($CFL = 2.0$).

(b) MATD model ($CFL = 2.0$).

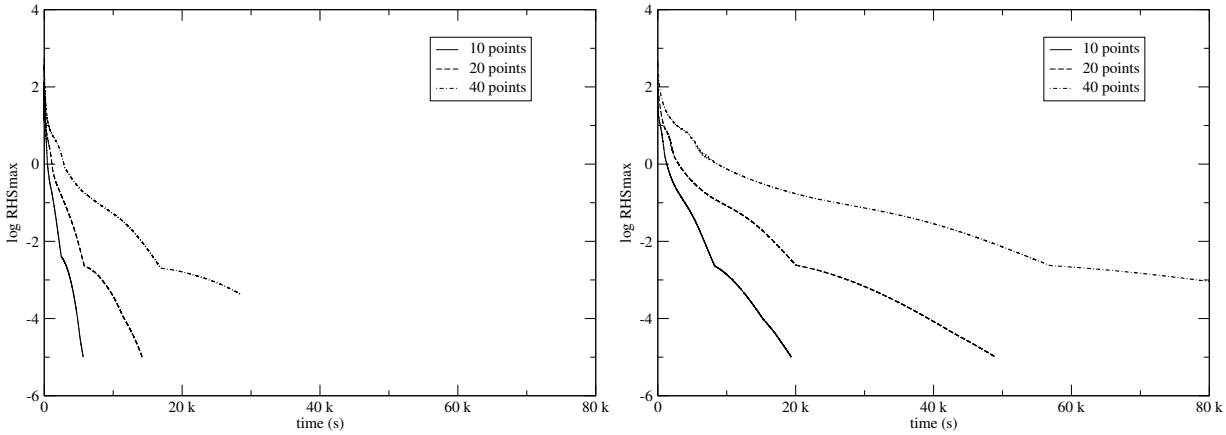

(c) CUSP model ($CFL = 2.0$).

(d) fROE scheme ($CFL = 1.5$).

Figure 5: Residue histories obtained with different flux computation schemes and meshes over the flat plate configuration.

the numerical diffusion into the computational code for the centred scheme.

Comparisons of numerical boundary layers for a zero-pressure gradient flat plate laminar flow with the corresponding theoretical Blasius solution show the level of accuracy that can be obtained with the present formulation. It is observed that the scalar artificial dissipation model presents a very large dependency on the grid density and topology. For this model, about 40 cells inside the boundary layer are required to correctly solve the boundary layer flow. The MATD model, as well as the CUSP and the Roe schemes, require only 10 points to achieve the same level of accuracy. Grid topology-independent converged solutions for all methods, however, are very close to the theoretical Blasius solution.

These schemes are also compared in terms of computational resource usage. It is observed that larger computational times are required for MATD, CUSP and fROE schemes when compared to the MAVR model. Nevertheless, such schemes keep the solution accuracy with successively less refined meshes, which is not observed with the MAVR model. Finally, the present results corroborate the initial assertive that grid density and topology have a strong influence in both numerical solution accuracy and convergence. Suitable grid configurations and flux computation schemes are presented in this work to which computational results and convergence are acceptable.

8. Acknowledgments

The authors would like to acknowledge Conselho Nacional de Desenvolvimento Científico e Tecnológico, CNPq, which partially supported the project under the Integrated Project Research Grant No. 501200/2003-7.

9. References

Allmaras, S., 2002, Contamination of Laminar Boundary Layers by Artificial Dissipation in Navier-Stokes Solutions, "Proceedings of the Conference on Numerical Methods in Fluid Dynamics", Reading, England, UK.

Azevedo, J. L. F., 1992, On the Development of Unstructured Grid Finite Volume Solvers for High Speed Flows, Report NT-075-ASE-N/92, Instituto de Aeronáutica e Espaço, S. J. Campos, SP.

Azevedo, J. L. F., Figueira da Silva, L. F., and Strauss, D., 2001, Order of Accuracy Study of Unstructured Grid Finite Volume Upwind Scheme, "Paper submitted to the Int. J. Numer. Meth. Fluids", Vol. .

Azevedo, J. L. F., Strauss, D., and Figueira da Silva, L. F., 1999, An Order of Accuracy Analysis for Flux-Vector Splitting Schemes on Unstructured Grids, "Proceedings of the 15th Brazilian Congress of Mechanical Engineering - COBEM 99", Águas de Lindóia, SP, Brazil.

Barth, T. J. and Jespersen, D. C., 1989, The Design and Application of Upwind Schemes on Unstructured Meshes, "27th AIAA Aerospace Sciences Meeting", AIAA Paper No. 89-0366, Reno, NV.

Bigarella, E. D. V., 2002, Three-Dimensional Turbulent Flow Simulations over Aerospace Configurations, Master's thesis, Instituto Tecnológico de Aeronáutica, São José dos Campos, SP, Brazil.

Bigarella, E. D. V., Basso, E., and Azevedo, J. L. F., 2003, Multigrid Adaptive-Mesh Turbulent Simulations of Launch Vehicle Flows, "Proceedings of the 21st AIAA Applied Aerodynamics Conference", AIAA Paper No. 2003-4076, Orlando, FL, USA.

Bigarella, E. D. V., Basso, E., and Azevedo, J. L. F., 2004, Centered and Upwind Multigrid Turbulent Flow Simulations with Applications to Launch Vehicles, "22nd AIAA Applied Aerodynamics Conference and Exhibit", AIAA Paper No. 2004-5384, Providence, RI. (to appear).

Fletcher, C. A. J., 1988, "Computational Techniques for Fluid Dynamics 2. Specific Techniques for Different Flow Categories", chapter 6, pp. 203–209. Springer-Verlag.

Hirsch, C., 1991, "Numerical Computation of Internal and External Flows Volume 2: Computational Methods for Inviscid and Viscous Flows", Wiley, Chichester.

Jameson, A., 1995a, Analysis and Design of Numerical Schemes for Gas Dynamics 1. Artificial Diffusion, Upwind Biasing, Limiters and Their Effect on Accuracy and Multigrid Convergence, "International Journal of Computational Fluid Dynamics", Vol. 4, pp. 171–218.

Jameson, A., 1995b, Analysis and Design of Numerical Schemes for Gas Dynamics 2. Artificial Diffusion and Discrete Shock Structure, "International Journal of Computational Fluid Dynamics", Vol. 5, pp. 1–38.

Jameson, A., Schmidt, W., and Turkel, E., 1981, Numerical Solution of the Euler Equations by Finite Volume Methods Using Runge-Kutta Time-Stepping Schemes, "Proceedings of the AIAA 14th Fluid and Plasma Dynamics Conference", AIAA Paper No. 81-1259, Palo Alto, CA.

Mavriplis, D. J., 1988, Multigrid Solution of the Two-Dimensional Euler Equations on Unstructured Triangular Meshes, "AIAA Journal", Vol. 26, No. 7, pp. 824–831.

Mavriplis, D. J., 1990, Accurate Multigrid Solution of the Euler Equations on Unstructured and Adaptive Meshes, "AIAA Journal", Vol. 28, No. 2, pp. 213–221.

Menter, F. R. and Grotjans, H., 1998, Application of Advanced Turbulence Models to Complex Industrial Flows, "Second International Conference on Advances in Fluid Mechanics", Udine, Italy.

Roe, P. L., 1981, Approximate Riemann Solvers, Parameter Vectors, and Difference Schemes, "Journal of Computational Physics", Vol. 43, No. 2, pp. 357–372.

Scalabrin, L. C., 2002, Numerical Simulation of Three-Dimensional Flows over Aerospace Configurations, Master's thesis, Instituto Tecnológico de Aeronáutica, São José dos Campos, SP, Brazil.

Spalart, P. R. and Allmaras, S. R., 1992, A One-Equation Turbulence Model for Aerodynamic Flows, "30th AIAA Aerospace Sciences Meeting and Exhibit", AIAA Paper No. 92-0439, Reno, NV.

Swanson, R. C. and Radespiel, R., 1991, Cell Centered and Cell Vertex Multigrid Schemes for the Navier-Stokes Equations, "AIAA Journal", Vol. 29, No. 5, pp. 697–703.

Swanson, R. C., Radespiel, R., and Turkel, E., 1998, On Some Numerical Dissipation Schemes, "Journal of Computational Physics", Vol. 147, No. 2, pp. 518–544.

Turkel, E. and Vatsa, V. N., 1994, Effect of Artificial Viscosity on Three-Dimensional Flow Solutions, "AIAA Journal", Vol. 32, No. 1, pp. 39–45.

van Leer, B., 1979, Towards the Ultimate Conservative Difference Scheme. V. A Second-Order Sequel to Godunov's Method, "Journal of Computational Physics", Vol. 32, pp. 101–136.

Zingg, D. W., De Rango, S., Nemec, M., and Pulliam, T. H., 1999, Comparison of Several Spatial Discretizations for the Navier-Stokes Equations, "14th AIAA Computational Fluid Dynamics Conference", AIAA Paper No. 99-3260, Norfolk, VA.